nature COMMUNICATIONS

ARTICLE

DOI: 10.1038/s41467-018-06320-z OPEN

Controlling factor of incoming plate hydration at the north-western Pacific margin

Gou Fujie[1], Shuichi Kodaira[1], Yuka Kaiho[1], Yojiro Yamamoto[1], Tsutomu Takahashi[1], Seiichi Miura[1] & Tomoaki Yamada[2]

Hydration of the subducting oceanic plate determines the amount of water transported from Earth's surface into its interior, and plate bending-related faulting (bend faulting) just prior to subduction is considered to promote hydration. Bend faulting shows significant spatial variation, but its contribution to hydration is still poorly understood. Here we present the results of controlled-source seismic surveys around the junction of the Japan and Kuril trenches. We found structural changes caused by bend faulting before subduction differed distinctly between both trenches and were well correlated with plate hydration after subduction, suggesting the bend faulting controls spatial variations in plate hydration. Differences in bend faulting are closely related to the angle between the current trench and the ancient spreading ridge, and the hydration is more extensive where this trench-ridge angle is oblique in the study area. Thus, we propose this angle is a major factor controlling plate hydration.

[1] Japan Agency for Marine-Earth Science and Technology (JAMSTEC), 3173-25, Showa-machi, Kanazawa-ku, Yokohama, 236-0001 Kanagawa, Japan. [2] Earthquake Research Institute, University of Tokyo, Yayoi 1-1-1, Bunkyo-ku, 113-0032 Tokyo, Japan. Correspondence and requests for materials should be addressed to G.F. (email: fujie@jamstec.go.jp)

As a part of global mantle convection, water is transported by subducting oceanic plates from Earth's surface into its interior, and the degree of hydration of the subducting oceanic plate determines the amount of transported water. In subduction zones, dehydration occurring within the subducting oceanic plate induces intra-slab intermediate-depth earthquakes, and the expelled water leads to arc magmatism, promotes metamorphism, lowers the slab temperature, and consequently affects interplate coupling[1,2]. Thus, the degree of hydration of the oceanic plate before subduction is key to understanding these subduction zone phenomena as well as the global water cycle.

The first-order control on oceanic plate hydration has previously been considered to be hydrothermal circulation and alteration at the spreading ridge. Recently, seismic and electromagnetic structure studies in subduction zones around the world have revealed that plate bending-related normal faulting near the subduction trench also promotes hydration of the oceanic plate[3-11]. Unlike hydrothermal circulation near the spreading ridge, which is confined to the oceanic crust, bend faulting near the subduction trench can potentially cut across the entire crust and reach to the upper mantle (e.g., the 1933 Sanriku earthquake[12,13]). Thus, if bend faults act as pathways for water penetration into the mantle, the amount of water transported by the oceanic plate might be much larger than previously thought[14,15].

Bend faulting shows remarkable variation among subduction trenches. However, the actual contribution of bend faulting and its spatial variations to plate hydration remains poorly understood because plate hydration is affected by various hydration and dehydration processes from the spreading ridge to the subduction trench and isolating the contribution of each process is not straightforward.

At the north-western Pacific margin off Japan, the old oceanic Pacific plate, which formed at 120–130 Ma at a fast-spreading ridge, is subducting beneath the north-eastern Japan arc at the junction of the Japan and Kuril trenches[16]. Although the same oceanic plate is subducting with a similar curvature at each trench, horst and graben structures, which are seafloor topographic features related to bend faulting, exhibit remarkable differences between the trenches (Fig. 1). In the Japan Trench, the throw of the bend faults is more than 800 m, and the fault spacing (horizontal distance between two horsts) is 10–15 km (Fig. 2c). In contrast, in the Kuril Trench, the throw is less than half (at most 400 m), and the spacing is much less (roughly 5 km) (Fig. 2d). These differences make this trench junction a good place to investigate the contribution of bend faulting and its spatial variations to plate hydration.

In this study, we show the seismic structural changes caused by bend faulting before subduction are well correlated with plate hydration after subduction. Differences in bend faulting between these two trenches are closely related to the angle between the current trench axis and the ancient spreading ridge axis. These findings indicate that the trench-ridge angle is a major controlling factor of plate hydration in these subduction zones.

Results

Tomographic imaging. To reveal the structural changes caused by bend faulting, we conducted extensive seismic surveys in the outer trench areas of these subduction zones (Fig. 1). We deployed Ocean Bottom Seismometers (OBSs) at intervals of 6 km along each survey line, and fired a large airgun array at 200-m intervals for OBSs and at 50-m intervals for a 6-km-long, 444-channel hydrophone streamer. The data quality was good (Supplementary Figs. 1-3). We succeeded in obtaining P-wave velocity (V_p) and S-wave velocity (V_s) models by tomographic traveltime inversion of both OBS and MCS data (see Methods).

The resultant V_p models show a simple layered oceanic plate structure in which the oceanic crust is 7 km thick (Fig. 3). The topmost mantle V_p outside of the bend faulting area was ~8.5 km s^{-1} in the Kuril Trench profile (A2) but ~7.9 km s^{-1} in the Japan Trench profile (A3). This large difference is well explained by seismic anisotropy due the alignment of olivine crystals in response to mantle flow at the spreading-ridge axis[17,18] and is not relevant to the bend faulting. On the other hand, the reduction of V_p and increase of the V_p/V_s ratio in the vicinity of the trench axis are considered to be related to the bend faulting (Fig. 3, Supplementary Figs 4-8). A reduction of V_p is widely observed in the outer trench area of subduction

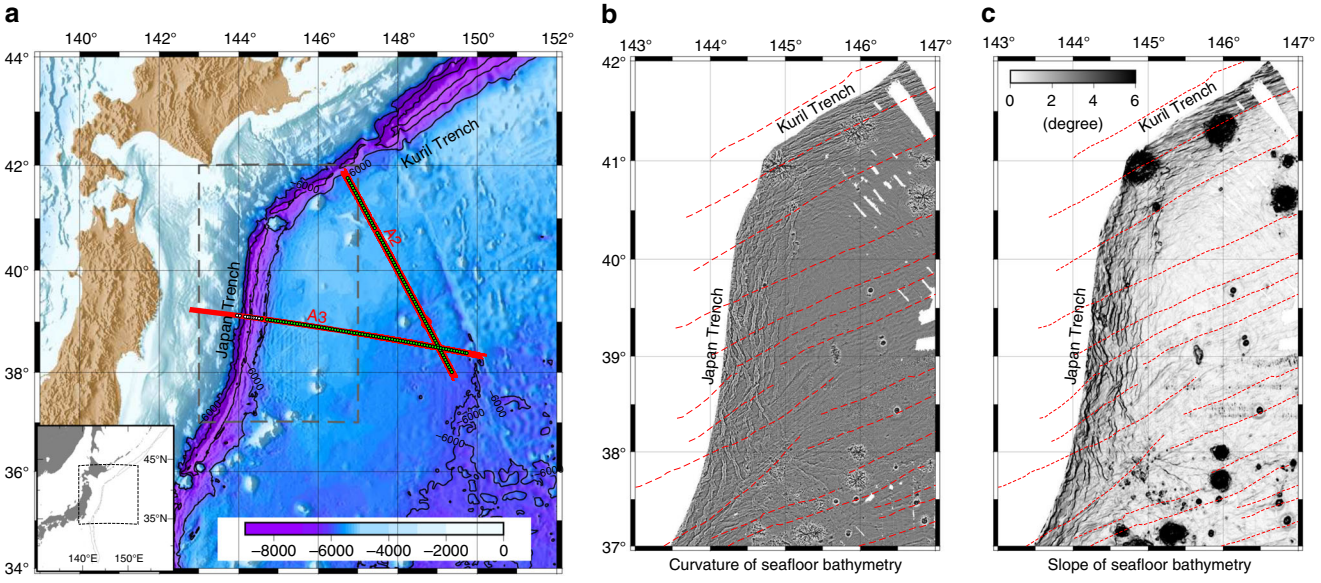

Fig. 1 Study area. **a** Bathymetric map of the north-western Pacific margin off Japan around the junction of Kuril and Japan trenches (location in inset). Solid red lines A2 and A3 are seismic survey lines. White circles represent OBSs located in the vicinity of the Japan Trench axis, and green circles represent other OBSs. No OBSs were deployed in the vicinity of the Kuril Trench axis. **b** Curvature (Laplacian) of the seafloor topography in the outer trench area. **c** Slope gradient of the seafloor in the outer trench area. Dashed red lines in **b**, **c** are magnetic anomaly lineations[16]

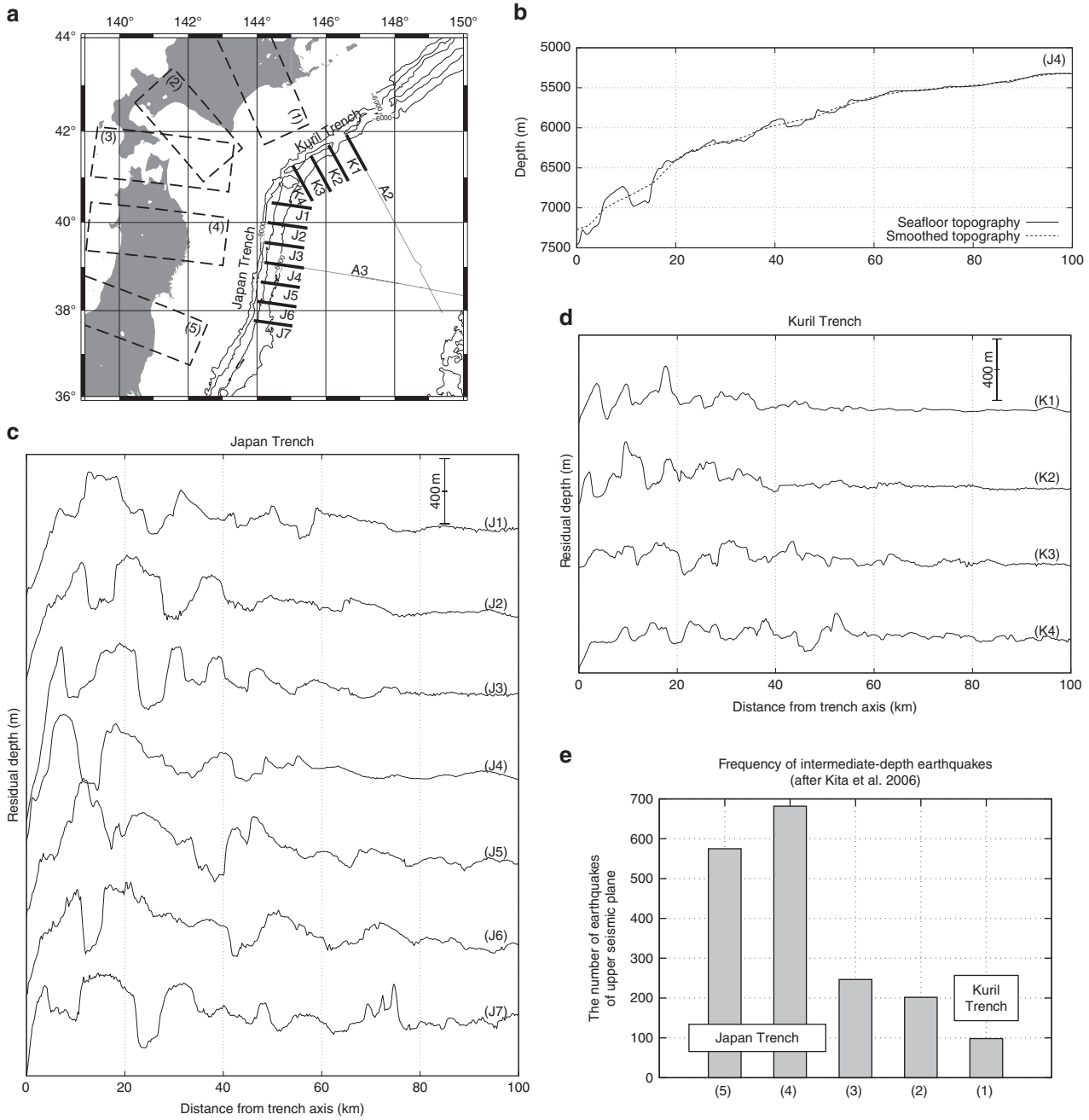

Fig. 2 Seafloor topography. **a** Location map. Solid lines K1-K4 and J1-J7 are the locations of the seafloor topographic profiles shown in **b**–**d**, and boxes 1-5 are the areas for evaluating the frequency of the earthquakes in **e**. **b** Seafloor topography along profile J4: raw data (solid) and smoothed data (dashed). Smoothing was performed with a moving average spatial filter. **c** Seafloor topography after removing the trend, defined by difference between raw and smoothed data, in the Japan Trench. The horizontal axis is the distance from the trench axis. The throw of horst and graben reaches more than 800 m near the trench axis. **d** Seafloor topography after removing the trend in the Kuril Trench. The throw is <400 m. **e** Frequency of dehydration-induced intermediate-depth earthquakes after subduction[24]. The number of earthquakes was calculated for each box (1)–(5). The vertical axis shows the peak of the upper plane earthquake frequency. The activity of dehydration-induced earthquakes is remarkably higher in the Japan Trench than in the Kuril Trench

zones worldwide, where it is interpreted to be a consequence of fracturing, water penetration, and hydration[5,6,8,10,19]. A reduction of V_p in the continental rifting area is similarly interpreted to be related with the water penetration and hydration caused by active faulting[20]. The increase of the V_p/V_s ratio strongly suggests an increase in water content, because V_s is more sensitive to the presence of water and hydrated minerals than V_p. Although we could not constrain the V_p/V_s ratio within the mantle owing to heavy attenuation of S-wave refraction from the mantle, the increase of the V_p/V_s ratio within the crust indicates that the water content became higher in the bend faulting areas. Therefore, we considered the V_p reduction to be accompanied by hydration as in other subduction zones and rifting areas.

Spatial variations in bend faulting and plate hydration. Structural changes related to bend faulting were commonly observed in

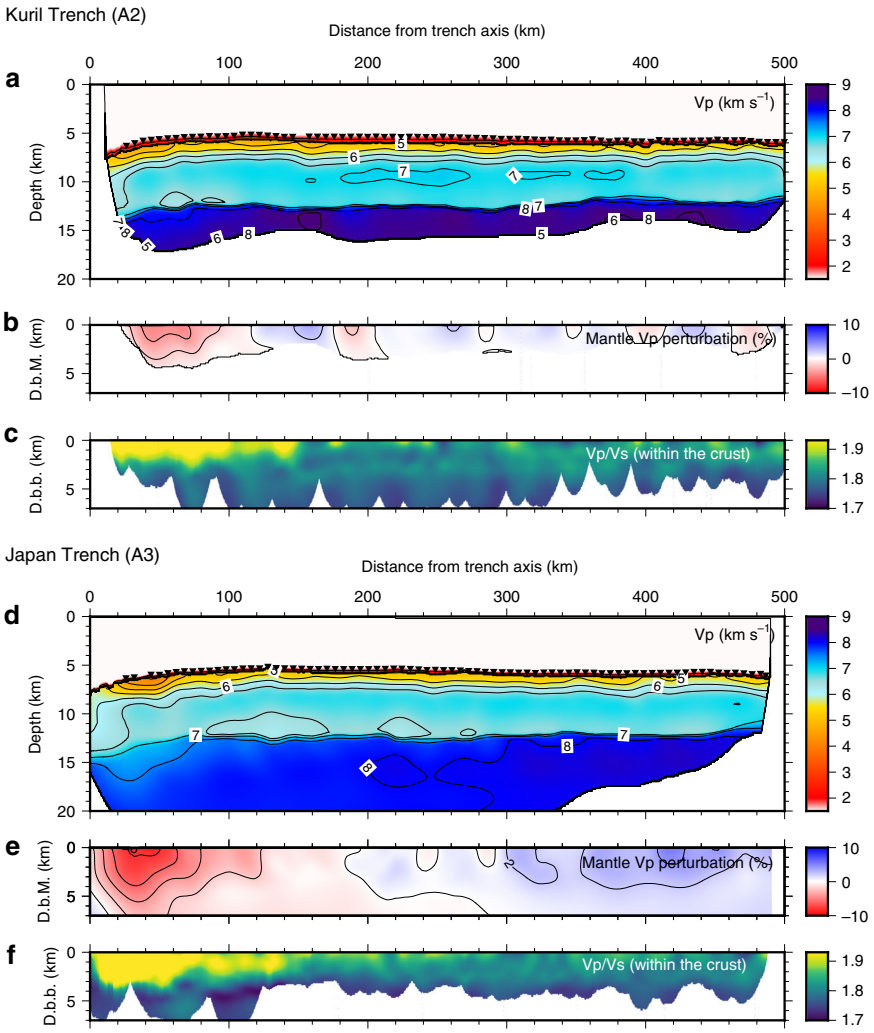

Fig. 3 Seismic velocity models derived from traveltime data of controlled-source seismic surveys. **a**–**c** V_p, V_p perturbation within the mantle, and the V_p/V_s ratio within the crust along the Kuril Trench profile. **d**–**f** V_p, V_p perturbation within the mantle, and the V_p/V_s ratio within the crust along and the Japan Trench profile. The inverted triangles in **a** and **d** show OBS locations. D.b.M. is depth below the Moho, and D.b.b. is depth below the basement. To enable direct comparisons between the trenches, only the OBSs shown by green circles in Fig. 1 were used to develop these velocity models. Results obtained by using all OBSs are shown in Supplementary Fig. 6. The reduction of mantle V_p become significant near the trench along both lines, which is well correlated with the development of normal faults (Supplementary Fig. 3b). The increase of V_p/V_s ratio within the crust starts at about 150 km from the trench axis and are well correlated with the roughness (continuity) of the basement reflection (Supplementary Fig. 3c), suggesting fracturing at the basement promotes water penetration into the oceanic crust[10]

both trenches, but the magnitude of the changes was not the same. First, the V_p reduction penetrates several times deeper in the Japan Trench than in the Kuril Trench; for example, a 2% V_p reduction reaches 7 km below the Moho in the Japan Trench but only 2 km below in the Kuril Trench, suggesting that the volume of altered mantle is several times larger in the Japan Trench than in the Kuril Trench. Second, the reduction rate of mantle V_p near the trench reaches ~12% in the Japan Trench, but no more than 8% in the Kuril Trench. Provided all of the mantle V_p reduction is caused by serpentinization and that the reduction rate is not dependent on seismic anisotropy, the degree of serpentinization can be roughly estimated to be 25% (water content ~3wt%) in the Japan Trench, and at most 15–20% (water content ~2wt%) in the Kuril Trench[21,22]. If the V_p reduction rate is considered in combination with the penetration depth in the mantle, mantle hydration is much larger in the Japan Trench than in the Kuril Trench. In addition, the thicker high-V_p/V_s layer in the Japan Trench also supports the inference that more water penetrates into the oceanic plate in the Japan Trench than in the Kuril Trench. Thus, our seismic velocity models indicate that plate hydration before subduction is remarkably higher in the Japan Trench than in the Kuril Trench.

The degree of plate hydration after subduction is often evaluated by the dehydration-induced intermediate-depth earthquakes activity occurring within the subducting oceanic plate[19,23]. In Japan, a dense nationwide seismic network has revealed the detailed distribution of intermediate-depth earthquakes in these subduction zones[24]. There are two seismic planes in this area and upper plane earthquakes occur mostly in the subducting oceanic crust and the topmost mantle. Upper plane seismic activity in the Japan Trench subduction zone is 5–6 times that in the Kuril Trench subduction zone (Fig. 2e), suggesting that the subducting oceanic plate is much more hydrated at the Japan Trench than at the Kuril Trench.

The good agreement between plate hydration before subduction, revealed by our seismic structure models, and plate

hydration after subduction, revealed by the frequency of dehydration-induced earthquakes, indicates that spatial variations in plate hydration are controlled primarily by the spatial variations in bend faulting in this subduction zone.

Discussion

The differences in bend faulting between these two trenches are attributable to differences in the type of bend faulting. Generally, there are two types of bend faults: reactivated abyssal-hill faults and newly created faults[25,26]. When an oceanic plate is formed at an oceanic spreading ridge, abyssal-hill faults are created parallel to the spreading axis. At intermediate- and fast-spreading ridges, abyssal-hill faults reach depths 3–5 km below the seafloor[26] and they are spaced a few kilometers apart[27]. Ancient abyssal-hill faults are considered to be weak zones, and they are easily reactivated if the bending axis (i.e., the trench axis) is subparallel to the abyssal-hill fabric (i.e., the ancient spreading ridge axis). Compilations of the world's subduction trenches[25,26] show that abyssal-hill faults are reactivated when the trench-ridge angle α is <25–30°; otherwise bend faults are newly created that cross pre-existing abyssal-hill faults.

In the north-western Pacific margin (Fig. 1), the abyssal-hill fabric is subparallel to the Kuril Trench (α~10°), but oblique to the Japan Trench (α=60–70°). Thus, the bend faults at the Kuril Trench are reactivated abyssal-hill faults whereas those at the Japan Trench are newly created faults. On the outer slope of the Kuril Trench, the strike and spacing of the bend faults are consistent with those expected for reactivated abyssal-hill faults. On the other hand, at the Japan Trench, the bend faults are subparallel to the bending axis (trench axis) and intersect the abyssal-hill fabric; as a result, the fault network consists of both new faults and ancient faults. This network of damaged and weak zones might promote more water penetration into the oceanic plate than the isolated faults at the Kuril Trench, and may be a plausible explanation for the differences in plate hydration between these subduction zones.

Compared with the reactivation of abyssal-hill faults, the formation of new faults is considered to be more difficult. Thus, there will be a concentration of extensional stress around a newly formed fault. The spacing between newly formed faults in the Japan Trench is at least twice that between reactivated faults in the Kuril Trench (Fig. 2), indicating that the magnitude of the plate bending-related extensional stress concentrated around each bend fault in the Japan Trench is at least twice that around the reactivated faults in the Kuril Trench. This result is consistent with the differences in the cumulative displacement of the bend faults between these trenches. The stress concentration in the Japan Trench facilitates the occurrence of large, normal faulting earthquakes cutting across the entire oceanic crust, which are essential for mantle hydration. Thus, a newly formed fault promotes mantle hydration much more effectively and the type of bend faulting, that is, the trench-ridge angle α, can therefore be considered a key controlling factor of plate hydration in the north-western Pacific margin.

A relationship between the trench-ridge angle α and plate hydration has been observed at the Alaska and the Middle American Trenches[19,28]. In both these subduction zones, the trench axes are nearly straight but the incoming oceanic plates, which have undergone reorganization, show remarkable along-trench segmentation. Plate hydration after subduction is larger along reactivated abyssal-hill fault segments (α < 25°) than along segments where α > 30°. These observations seemingly contradict findings in the north-western Pacific margin; however, the along-trench variations in plate hydration in these subduction zones can also be explained by the development of bend faulting. Reactivated bend faults are clearly observed in the segments where α < 25°, but almost no bend faulting can be recognized in the segments where α > 30°; thus, in these subduction zones, plate hydration is dependent on the development of bend faulting. The lack of bend faults in segments where α > 30° in these subduction zones can be explained by (1) difficulties in forming new faults because the plate curvature is significantly smaller than that in the north-western Pacific margin, and (2) relatively younger plate ages which might influence the rigidity and flexibility of the oceanic plate. In addition, we cannot exclude the possibility that along-trench variations in plate hydration are related to pre-existing tectonic features, because in these subduction zones each plate segment has a very different tectonic history.

Our seismic surveys around the junction of the Japan and Kuril trenches have revealed that subducting plate hydration is strongly dependent on plate bending-related faulting prior to subduction. Differences in plate hydration can be explained by the type of bend faulting; plate hydration is more effective where the faults are newly formed than where they are reactivated abyssal-hill faults. The type of bend faulting is dependent on α, the angle between the current trench axis and the ancient spreading ridge axis. Thus, we propose that the trench-ridge angle is a key controlling factor of the spatial variations in plate hydration in the north-western Pacific margin. However, spatial variations in plate hydration are also likely to be affected by other structural features such as plate curvature, plate age, and the presence of transform faults on the oceanic plate. Further, we need additional information, such as electric resistivity measurements, to quantitatively assess water transport by the oceanic plate. A broader range of studies will be essential to reveal the details of water transport by subducting oceanic plates.

Methods

Data acquisition. We deployed 80 Ocean Bottom Seismometers (OBSs) along line A2 (Kuril Trench) and 86 OBSs along line A3 (Japan Trench) at a spacing of 6 km and fired a large airgun array (total volume 7800 cubic inches) from R/V Kairei at 200-m intervals for OBSs and at 50-m intervals for a 444-channel, 6-km-long hydrophone streamer. In OBS vertical component data, we observed good quality P-wave refractions from the oceanic crust and mantle, and good quality wide-angle reflections from the Moho discontinuity (Supplementary Figs 1, 2). In addition, we observed S-wave refractions and reflections in the radial (horizontal) component data. On time-migrated multi-channel seismic reflection sections, we could trace the basement (top of the oceanic crust) and the Moho clearly except in the areas with bend faults (Supplementary Fig. 3).

Data processing. We modeled V_p and V_s structures by a tomographic traveltime inversion method[10,29]. For V_p modeling, we divided seismic structure models into four layers (seawater, sediment, crust, and mantle) separated by three interfaces (seafloor, basement, and Moho) and determined V_p by using crustal and mantle refractions and Moho reflections in OBS data, and two-way traveltimes from the basement and Moho in multi-channel seismic data (Fig. 3, Supplementary Figs. 4, 5).

To model V_s and the V_p/V_s ratios, we utilized P-to-S conversion phases as well as P-waves. In our study area, the most efficient P-to-S conversion interface was considered to be the sediment basement. We therefore assumed that large-amplitude P-to-S phases were converted at the basement. Generally, there are two P-to-S conversions: P-to-S conversion of the ascending ray (PPS) and P-to-S conversion of the descending ray (PSS). The PPS is converted just beneath each OBS and has almost the same apparent velocity as P. The PSS is converted just beneath the airgun shot point and has the apparent S-wave velocity of the crust. The PPS can effectively constrain V_s within the sediments, and the PSS can effectively constrain V_s below the sediment basement.

Unlike P-wave mantle refractions, S-wave mantle refractions were not clearly observed in the horizontal data (radial component) near the trench axis where bend faults are well developed (Supplementary Figs 1a, 2a). Thus, we focused on the crustal structure and adopted three-layer model parameterization (seawater, sediment, and crust) to develop the V_s and V_p/V_s ratio models. We adopted the following 3-step inversion scheme to determine V_s models. First, we determined the V_p structure by tomographic traveltime inversion using first arrivals and multi-channel seismic two-way reflection traveltimes from the basement. Second, we modeled V_s within the sediment by traveltime inversion using only the PPS phases.

Finally, we modelled V_s beneath the basement by tomographic inversion using PSS phases. We calculated the V_p/V_s ratio directly from these V_p and V_s models.

Uncertainty of the obtained models. Inversion results are generally dependent on the starting models as well as on the data. We evaluated the dependency by a Monte Carlo approach[29–31] as follows. First, we constructed a wide range of starting models randomly. Then, we applied tomographic traveltime inversion to all starting models to determine the final seismic velocity models. Finally, we calculated the average model and its standard deviation (SD). We considered the SD to be the uncertainty of the obtained seismic velocity models.

The random parameters for the starting V_p models were V_p, V_p gradient, and layer thickness. The starting model for V_s inversion was generated from each final V_p model by assuming a V_p/V_s ratio of 8.0 in the sediment and 1.75 below the basement. In both V_p and V_s modeling, we generated 400 final models that fulfilled the condition $\chi^2 < 1$, where χ^2 is the normalized sum of the root mean square of traveltime misfits divided by the uncertainty of each traveltime pick. Then, we calculated the average V_p models (Fig. 3) and their SDs (Supplementary Figs 4-6).

The SD of the final V_p and V_s models within the oceanic upper crust and topmost mantle was usually less than 0.1 km s^{-1} except at the two ends of the models. The SD of the final V_p within the topmost mantle became a little larger near the trench axis, but it was still usually <0.2 km s^{-1}, indicating that the differences we found in V_p reduction between the Kuril Trench and the Japan Trench were significant. On the other hand, we could not discuss the details of lower crustal V_p because the SD of lower crust was relatively large. This is because the trade-off between the lower crustal V_p and the Moho depth (crustal thickness) were not well constrained by our data.

In addition to the uncertainty analysis, we applied checkerboard resolution tests (CRT) to evaluate the spatial resolution of velocity perturbation (Supplementary Fig. 4-6). The checkerboard size is 30×3 km and we gave 5% perturbation. The checkerboard patterns were well recovered within the upper crust for both of V_p and V_s tomography and within the topmost mantle for V_p tomography, which suggest that the lateral velocity perturbations there are reliable at the scale of 30 km. On the other hand, especially in the Japan Trench (Line A3), the checkerboard patterns could not be well recovered within the lower crust for V_p tomography due to the lack of laterally propagating phases within the lower crust. Thus, we focus on the seismic velocity variations in the upper crust and the topmost mantle in this study.

Bathymetry data. Seafloor bathymetric data in Figs. 1 and 2 are ETOPO1, and a compilation of multi-narrow beam echo sounder data collected by Japan Coast Guard and JAMSTEC[32]. These figures were plotted using the Generi Mapping Tool software [33].

Data availability

All the seismic survey data can be requested from JAMSTEC crustal structural database site (https://www.jamstec.go.jp/jamstec-e/IFREE_center/index-e.html).

Received: 13 March 2018 Accepted: 22 August 2018
Published online: 21 September 2018

References

1. Hyndman, R. & Peacock, S. Serpentinization of the forearc mantle. *Earth Planet. Sci. Lett.* **212**, 417–432 (2003).
2. Rüpke, L. H., Morgan, J. P., Hort, M. & Connolly, J. A. D. Serpentine and the subduction zone water cycle. *Earth Planet. Sci. Lett.* **223**, 17–34 (2004).
3. Ranero, C. R., Morgan, J. P., Mcintosh, K. & Reichert, C. Bending-related faulting and mantle serpentinization at the Middle America trench. *Nature* **425**, 367–373 (2003).
4. Grevemeyer, I., Ranero, C. R., Flueh, E. R., Kläschen, D. & Bialas, J. Passive and active seismological study of bending-related faulting and mantle serpentinization at the Middle America trench. *Earth Planet. Sci. Lett.* **258**, 528–542 (2007).
5. Contreras-Reyes, E., Grevemeyer, I., Flueh, E. & Reichert, C. Upper lithospheric structure of the subduction zone offshore of southern Arauco peninsula, Chile, at 38S. *J. Geophys. Res.* **113**, B07303 (2008).
6. Ivandic, M., Grevemeyer, I., Bialas, J. & Petersen, C. Serpentinization in the trench-outer rise region offshore of Nicaragua: constraints from seismic refraction and wide-angle data. *Geophys. J. Int.* **180**, 1253–1264 (2010).
7. Goff, J. A. & Jordan, T. H. Stochastic modeling of seafloor morphology: Inversion of sea beam data for second-order statistics. *J. Geophys. Res.* **93**, 13589–13608 (1988).
8. Contreras-Reyes, E. et al. Deep seismic structure of the Tonga subduction zone: implications for mantle hydration, tectonic erosion, and arc magmatism. *J. Geophys. Res.* **116**, B11013 (2011).
9. Key, K., Constable, S., Matsuno, T., Evans, R. & Myer, D. Electromagnetic detection of plate hydration due to bending faults at the middle america trench. *Earth Planet. Sci. Lett.* **351**, 45–53 (2012).
10. Fujie, G. et al. Systematic changes in the incoming plate structure at the Kuril trench. *Geophys. Res. Lett.* **40**, 88–93 (2013).
11. Naif, S., Key, K., Constable, S. & Evans, R. L. Water-rich bending faults at the middle america trench. *Geochem. Geophys. Geosyst.* **16**, 2582–2597 (2015).
12. Kanamori, H. Seismological evidence for a lithospheric normal faulting - the Sanriku earthquake of 1933. *Phys. Earth Planet. Inter.* **4**, 289–300 (1971).
13. Uchida, N., Kirby, S. H., Umino, N., Hino, R. & Kazakami, T. The great 1933 sanriku-oki earthquake: reappraisal of the main shock and its aftershocks and implications for its tsunami using regional tsunami and seismic data. *Geophys. J. Int.* **206**, 1619–1633 (2016).
14. Peacock, S. Are the lower planes of double seismic zones caused by serpentine dehydration in subducting oceanic mantle? *Geology* **29**, 299 (2001).
15. Faccenda, M. Water in the slab: a trilogy. *Tectonophysics* **614**, 1–30 (2014).
16. Nakanishi, M. In *Accretionary Prisms and Convergent Margin Tectonics in the Northwest Pacific Basin*, Vol. 8 of *Modern Approaches in Solid Earth Sciences* (eds Ogawa, Y., Anma, R. & Dilek, Y.) 1–38 (Springer, Netherlands, 2011).
17. Kodaira, S. et al. Seismological evidence of mantle flow driving plate motions at a palaeo-spreading centre. *Nat. Geosci.* **7**, 371–375 (2014).
18. Miller, N. C. & Lizarralde, D. Finite-frequency wave propagation through outer rise fault zones and seismic measurements of upper mantle hydration. *Geophys. Res. Lett.* **43**, 7982–7990 (2016).
19. Shillington, D. J. et al. Link between plate fabric, hydration and subduction zone seismicity in Alaska. *Nat. Geosci.* **8**, 961–964 (2015).
20. Bayrakci, G. et al. Fault-controlled hydration of the upper mantle during continental rifting. *Nat. Geosci.* **9**, 384–388 (2016).
21. Carlson, R. & Miller, D. Mantle wedge water contents estimated from seismic velocities in partially serpentinized peridotites. *Geophys. Res. Lett.* **30**, 1250 (2003).
22. Christensen, N. Serpentinites, peridotites, and seismology. *Int. Geol. Rev.* **46**, 795–816 (2004).
23. Ranero, C., Villasenor, A., Morgan, J. & Weinrebe, W. Relationship between bend-faulting at trenches and intermediate-depth seismicity. *Geochem. Geophys. Geosyst.* **6**, Q12002 (2005).
24. Kita, S., Okada, T., Nakajima, J., Matsuzawa, T. & Hasegawa, A. Existence of a seismic belt in the upper plane of the double seismic zone extending in the along-arc direction at depths of 70–100 km beneath NE Japan. *Geophyps. Res. Lett.* **33**, L24310 (2006).
25. Masson, D. G. Fault patterns at outer trench walls. *Mar. Geophys. Res.* **13**, 209–225 (1991).
26. Billen, M., Cowgill, E. & Buer, E. Determination of fault friction from reactivation of abyssal-hill faults in subduction zones. *Geology* **35**, 819–822 (2007).
27. Macdonald, K., Fox, P., Alexander, R., Pockalny, R. & Gente, P. Volcanic growth faults and the origin of Pacific abyssal hills. *Nature* **380**, 125–129 (1996).
28. Van Avendonk, H. J. A., Holbrook, W. S., Lizarralde, D. & Denyer, P. Structure and serpentinization of the subducting Cocos plate offshore Nicaragua and Costa Rica. *Geochem. Geophys. Geosyst.* **12**, Q06009 (2011).
29. Fujie, G., Kodaira, S., Sato, T. & Takahashi, T. Along-trench variations in the seismic structure of the incoming pacific plate at the outer rise of the northern japan trench. *Geophys. Res. Lett.* **43**, 666–673 (2016).
30. Korenaga, J. et al. Crustal structure of the southeast Greenland margin from joint refraction and reflection seismic tomography. *J. Geophys. Res.* **105**, 21591–21614 (2000).
31. Sambridge, M. & Mosegaard, K. Monte carlo methods in geophysical inverse problems. *Rev. Geophys.* **40**, 3-1–3-29 (2002).
32. JHOD-Japan Coast Guard and JAMSTEC. Compilation of bathymetric data off Tohoku. *Seismol. Soc. Jpn News Lett.* **23**, 35–36 (2011).
33. Wessel, P. & Smith, W. New, improved version of generic mapping tools released. *EOS Trans.* **79**, 579 (1998).

Acknowledgements

We gratefully acknowledge the captain, crew and marine technicians of R/V Kairei. This study was partly supported by a KAKENHI grant (15H05718) from the Japan Society for the Promotion of Science.

Author contributions

G.F. and S.K. designed the seismic surveys. Y.K., Y.Y., G.F., and T.T., participated in the research cruises and collected seismic survey data. T.Y. provided ultra-deep OBSs and pre-processed the data. S.M. provided logisitcal support for seismic data acquisition and

processing. G.F. analyzed the seismic survey data and wrote the manuscript with contributions from all of the co-authors.

Additional information

Supplementary Information accompanies this paper at https://doi.org/10.1038/s41467-018-06320-z.

Competing interests: The authors declare no competing interests.

Reprints and permission information is available online at http://npg.nature.com/reprintsandpermissions/

Publisher's note: Springer Nature remains neutral with regard to jurisdictional claims in published maps and institutional affiliations.